Digest Journal of Nanomaterials and Biostructures Vol. 19, No. 2, April - June 2024, p. 875 - 887

Preparation of PANI/COF/ BiOBr composites and its photocatalytic degradation of organic compounds

J. H. Feng, S. Y. Li*, W. J. Li, W. H. He, D. M. Yao, X. L. Li
College of Chemical and Biological Engineering, Hechi University, Yizhou 546300, Guangxi Province, China

PANI/COF/BiOBr catalysts were synthesized by hydrothermal method basing on Schiff base reaction. The composites were characterized by XRD, SEM, etc., and at the same time, the photocatalytic property and degradation mechanism of PANI/COF/ BiOBr catalysts were studied by degrading organic simulated dyes. The experimental results showed that the main structure of PANI/COF/BiOBr composite was flower ball structure with BiOBr main crystal type of tetragonal phase, and the degradation rates of PANI/COF/BiOBr were 1.44, 1.55 and 1.47 times of pure BiOBr for Rhodamine B, methylene blue and tetracycline hydrochloride, respectively. The free radical quenching experiment showed that h^+ and e^- were the most active species in the photocatalytic process.

(Received March 15, 2024; Accepted June 12, 2024)

Keywords: BiOBr, photocatalytic degradation, COF, mechanism

1. Introduction

With the development of pharmaceutical and chemical industries, pollutants such as dyes and antibiotics have been released into the water environment, causing serious impacts on the ecosystem [1,2]. Organic dye wastewater and antibiotics are not easy to degrade and the traditional treatment methods are suboptimal, so the development of pollutants cleaning technology with efficient, wide range of application, low energy consumption, and strong oxidation capacity of pollutants is the goal that researchers have been pursuing. The photocatalytic technology developed in recent years has been widely concerned for its advantages of high efficiency, energy-saving, simple operation and catalytic degradation under sunlight, etc., and it is of great significance to explore the photocatalysts which has high degradation performance responding to broad spectrum and high charge separation efficiency for practical applications [3-5].

Two-dimensional BiOX(X=Cl, Br, I) is considered as a potential photocatalyst under visible light irradiation [6]. In the inherent two-dimensional layer structure, BiOBr, as a new type of semiconductor photocatalyst, has a suitable band gap energy (E_g=2.7eV), excellent photon capture ability and inherent electrostatic field, which can promote the separation of photogenerated carriers [7,8]. However, BiOBr still has some defects such as poor light capture capability. insufficient specific area of the photocatalyst and poor affinity with the pollutant, and also the high

* Corresponding author: lishengying05@163.com
https://doi.org/10.15251/DJNB.2024.192.875

recombination rate of photogenerated electron-hole pairs inhibiting the reaction efficiency [9,10]. In order to overcome these problems, several modification methods have been developed, including heterostructure construction [11,12], element doping [13,14], and vacancy defect construction [15,16]. Through the modification of these methods, good research results have been achieved.

Many studies have shown that the introduction of conductive polymers with non-local π-π conjugated structure can accelerate charge transfer and improve photocatalytic activity. Polyaniline (PANI) is a conductive polymer with delocalized π-π conjugated structure, which enables it to ensure high charge separation efficiency and high visible light capture ability in a wide wavelength range of 400-1200nm [17-19]. So far, many published studies have shown that the combination of polyaniline and semiconductor can improve the efficiency of carrier migration by polyanilines, expand the optical response region, and improve the efficiency of light utilization. Such as TiO_2-PANI[20], PANI/PbS QD[21]. The results of Z-scheme BiOBr-GO-polyaniline photocatalyst successfully synthesized by Qing et al. [22], and PANI/Bi_4O_5Br prepared by Xu et al. [23] showed that the presence of polyaniline can significantly expand the spectral response range. While it is beneficial to transfer electrons from the photocatalyst to the electron acceptor groups of organic pollutants, thus improving the photocatalytic performance.

Covalent organic framework (COFs) is a new type of organic porous polymer with low density, structural adjustability and regular pore structure. COFs have good crystallinity, which is conducive to charge transport and can inhibit carrier recombination [24]. In recent years, many researchers have carried out research on photocatalytic organic pollutants basing COF[25,26]. For example, Zhi et al. synthesized two new piperazine-linked COFs with fully conjugated structures and eclipsed π-stacking model, demonstrating enhanced photoinduced carrier transport and separation [27].

The above analysis inspired us to synthesize a new photocatalyst containing BiOBr, polyaniline and COF. PANI/COF/BiOBr was synthesized by hydrothermal method basing on Schiff base reaction with $Bi(NO_3)_3$ and hexadecyl trimethyl ammonium bromide (CTAB) as Bi source and Br source, respectively. To study the degradation efficiency on Rhodamine B, methylene blue and tetracycline hydrochloride, the photocatalytic properties of BiOBr and optimal composites were studied, and the mechanism of photocatalytic reaction was explored through quenching experiments.

2. Experimental

2.1. Preparation of COF

0.3mmol 2,4,6-triformylphloroglucinol and 0.45mmol 2-chloro-1,4-diaminobenzene were dissolved in 45ml dichloromethane and 15ml trichloromethane, and 0.45ml acetic acid was added to the above solution. The mixture was stirred in a water bath at 35℃ for 48 hours, and than the final solution was centrifugated at 5000rpm and washed with dichloromethane and ethanol. At last, it was dried at 60℃ for12h.

2.2. Preparation of BiOBr

0.75mmol CTAB and 0.75mmol $Bi(NO_3)_3 \cdot 5H_2O$ were added to 40mL glycol and stirred at

35℃ for 2 hours, after that the mixture was transferred to a reaction kettle and reacted at 180℃ for 6h. After the reaction, the product was washed with deionized water and ethanol several times and dried at 60℃ for 6h.

2.3. Preparation of BiOBr composites

0.75mmol CTAB and 0.75mmol $Bi(NO_3)_3 \cdot 5H_2O$ were added to 40mL glycol and the solution was stirred at 35℃ for 0.5 hours. After that 0.0114g COF and 0.0114g PANI were added (or 0.0114g PANI or 0.0114g COF). The solution continued to stir for 1.5 hours, and was transferred to the reactor, and reacted at 180℃ for 6h. After the reaction, the product of PANI/COF/BiOBr (PANI/ BiOBr or COF/BiOBr) was washed with deionized water and ethanol several times and dried at 60℃ for 6h. The preparation path of the composite PANI/COF/BiOBr was shown in Fig.1.

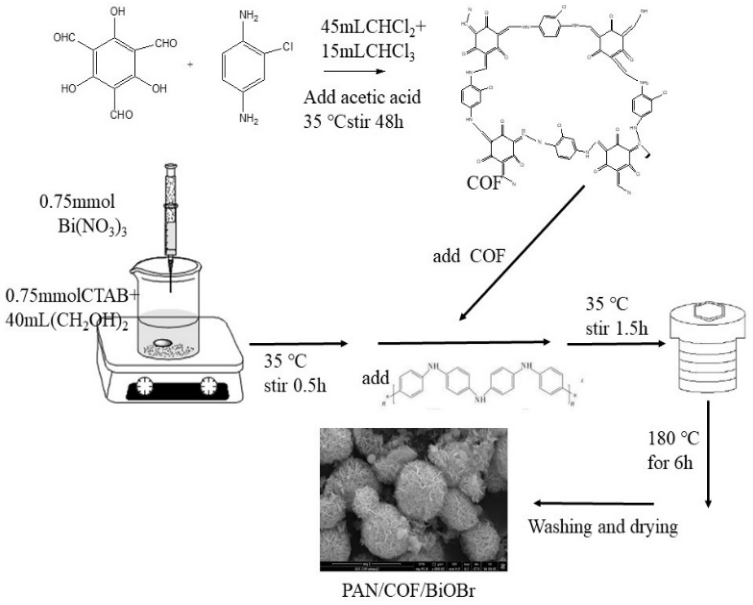

Fig. 1. The preparation path of PANI/COF/BiOBr composite.

2.4. Characterization of BiOBr composites

X-ray powder diffraction pattern(XRD) was obtained by a D/ Max 3B X-ray diffractometer (Japan) with Cu Kα irradiation source (λ=1.5418 Å) through the 2θ range from 5° to 90. Field Emission Environment Scanning Electron Microscope (FEI Quanta 200FEG, Dutch Philips) was used to test the morphologies of prepared samples. Fourier-transform infrared(FT-IR) spectra was characterized by Nicolet 6700(USA). The optical properties of the samples were characterized by a UV-2600 ultraviolet/visible diffuse reflectance spectrophotometer (DRS) The concentration of organic simulated dyes was obtained by Uv-Vis Spectrophotometer (model: 8453, Agilent, USA).

2.5. Photocatalytic performance of BiOBr composites

In the experiment, 0.05g catalyst was weighed and used to degrade 50mL of 80mg/L

Rhodamine B solution, 100mg/L methylene blue solution and 30mg/L tetracycline hydrochloride solution, respectively. The suspension was stirred at dark for 30 minutes to reach the adsorption equilibrium. After then, the simulated visible light (Xenon light source using cut-off 400 nm filter) was turned on for 120 minutes. A certain amount of solution was taken out every 30 min and filterd with 0.22 um microporous filter membrane to remove the catalysts. The photodegradable activity was observed by measuring the absorbance by Uv-Vis Spectrophotometer. The degradation rate (D%) was expressed as follows:

$$D\% = \frac{C_0 - C_t}{C_0} = \frac{A_0 - A_t}{A_0} \times 100\% \quad (3)$$

2.6. Cycle performance of BiOBr composites

After the photocatalytic experiment, the catalysts were transferred to centrifuge and separated. And then the catalysts were treated by 0.1mol/LNaOH, deionized water, 0.1mol/LHCl respectively , and washed to neutral, and then dried. The same photocatalytic reaction was carried out, and the catalyst was reused for three cycles to study its reusable performance.

2.7. Photocatalytic mechanism of BiOBr composites

Sodium oxalate, silver nitrate, p-benzoquinone and isopropyl alcohol solution were used as the quenching agents of photogenerated holes (h^+), photogenerated electrons (e^-), superoxide radicals ($\cdot O^{2-}$) and hydroxyl radicals ($\cdot OH$), respectively. On the basis of the photocatalytic experiment, 0.05g PANI/COF/BiOBr composite material was put into 50ml 80mg/L Rhodamine B solution, 5mL of the above-mentioned quencher with a concentration of 0.075mol /L and 5mL of distilled water as a blank control to investigate the role of free radicals in the photocatalytic process during the light process.

3. Results and discussion

3.1. Characterization of composites

3.1.1. XRD characterization of composites

XRD pattern of BiOBr composites was shown in Fig.1. It showed that the related diffraction peaks of 2θ at 25.01°, 32.23°, 32.48°, 39.69°, 46.52°, 56.34° and 57.20° were consistent with the peaks of the BiOBr standard card (PDF#85-0862), which were corresponding to crystal faces (101), (102), (110), (112), (200), (211) and (212) of the tetragonal phase structure of BiOBr . In addition, these peaks were sharp, indicating that the crystallinity of the sample was high, and it could be known that the main structure of the synthesized composite sample was BiOBr. COF had a strong diffraction peak at 27°, corresponding to its (001) crystal face. The peak locations of COF/BiOBr, PANI/BiOBr, PANI/COF/ BiOBr and pure BiOBr were roughly the same, indicating that the minor addition of PANI and COF did not change the main phase structure of the composite.

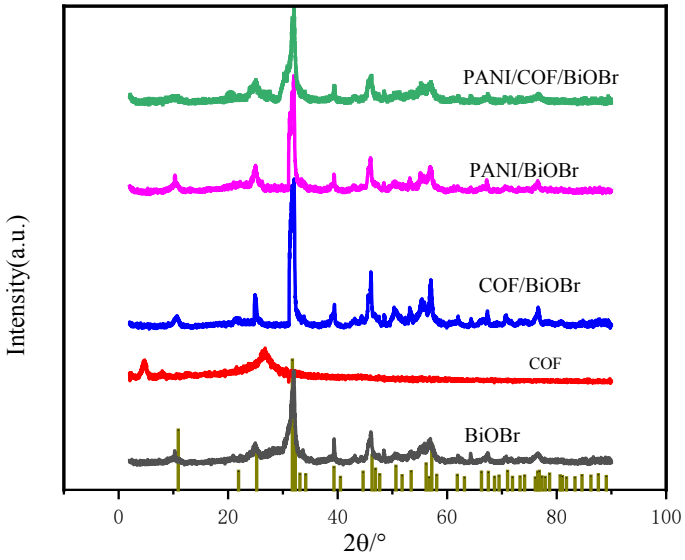

Fig. 2. XRD spectra of BiOBr composites.

3.1.2. FT-IR characterization of BiOBr composites

The infrared spectra of BiOBr composites was shown in Fig. 3. It showed that the infrared peak position of BiOBr and its composites could be observed to be roughly the same. The infrared characteristic peak of 3440.00cm^{-1} was the vibration absorption of water molecules adsorbed by the material. The peak at 520cm^{-1} was the characteristic peak of BiOBr material, corresponding to the existence of Bi-O bond stretching vibration peak [28]. The infrared spectra of BiOBr and its complexes both had the peak at 520cm^{-1}, confirming the existence of the main structure of BiOBr. In addition, the COF and the composites loaded COF all had the peak at 1455 cm^{-1}, possibly duing to the C-N bond of the COF material. The addition of PANI did not cause significant changes in the bonding of composites.

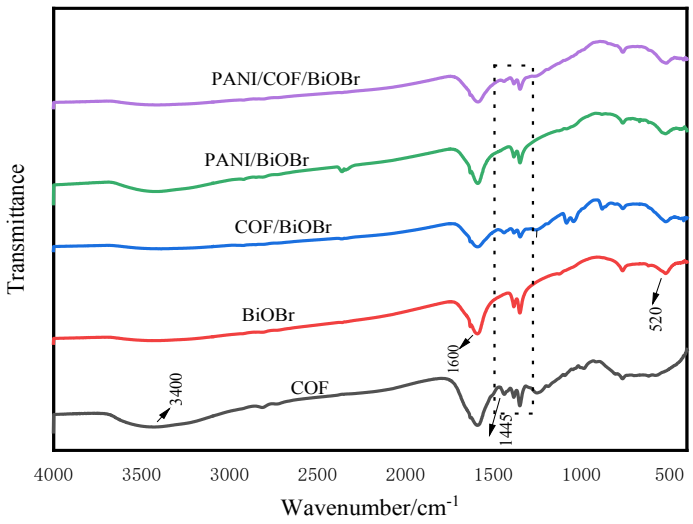

Fig. 3. Infrared spectra of BiOBr composites.

3.1.3. SEM characterization of BiOBr composites

SEM image of BiOBr composites was shown in Fig.4. It could be seen that the morphology of BiOBr and COF/BiOBr was irregular, with rough surfaces and uneven sizes from Fig.1 a and Fig1 b. A small number of flower-like spheres with irregular morphology was shown in Fig1 c, at the same time, the morphology of PANI/COF/BiOBr contained regular flower spheres which had a larger specific surface area, enabling the catalyst to contact with the reactants adequately, and improving the photocatalytic activity.

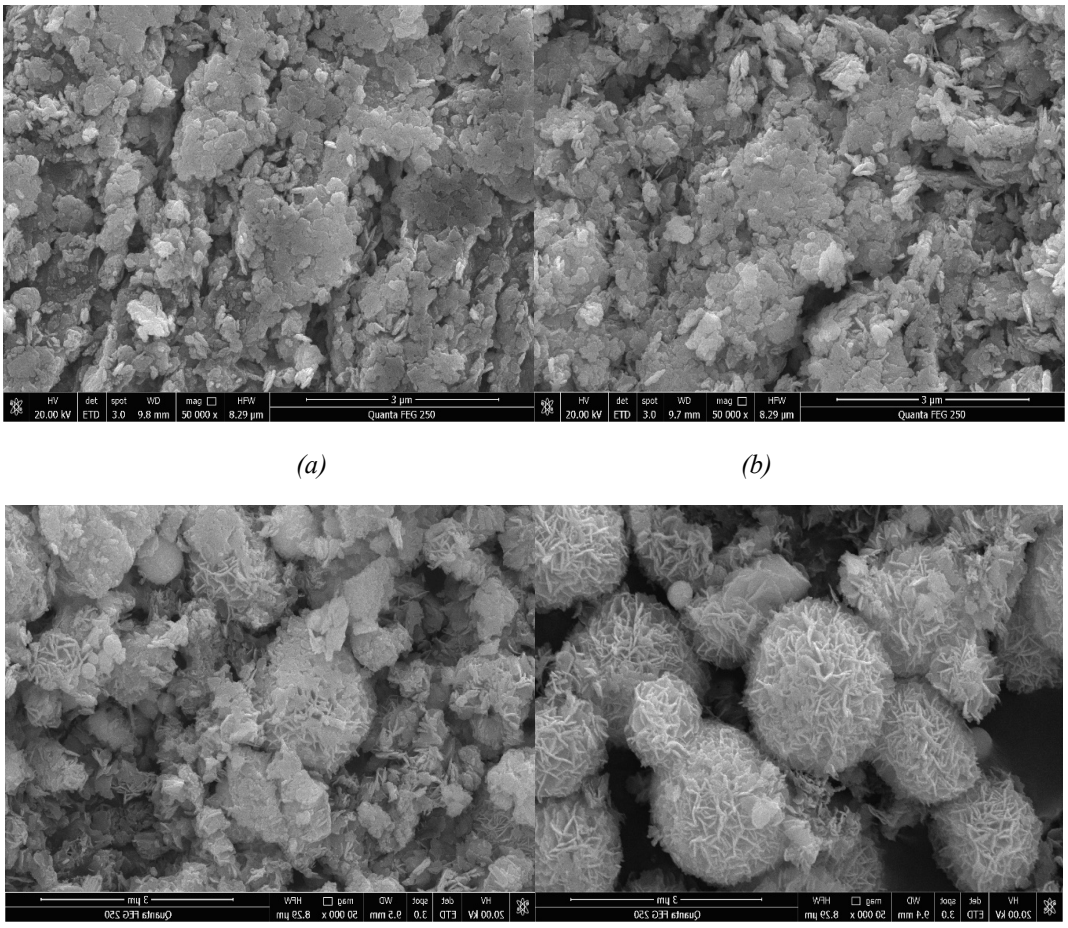

Fig. 4 SEM images of BiOBr composites (a) SEM image of BiOBr at 50000x; (b) SEM of COF/BiOBr at 50000x; (c) SEM image of PANI/BiOBr at 50000x; d. SEM image of PANI/COF/BiOBr at 50000x.

3.1.4. UV-Vis DRS characterization of BiOBr composites

The UV diffuse reflection of BiOBr composites was shown in Fig. 5. It showed that PANI/BiOBr had the weakest optical response before 400nm from Uv-vis absorption spectrum in 5 (a), and after 400nm, the spectral responses of BiOBr, COF/BiOBr, PANI/BiOBr and PANI/COF/BiOBr catalysts were enhanced successively, and the spectral responses of PANI/COF/BiOBr catalysts were the strongest. The optical bandgap of BiOBr, COF/BiOBr, PANI/BiOBr, PANI/COF/BiOBr catalysts was 2.95eV, 2.90eV, 2.64eV, 2.58eV by fitting the (αhv)

^{2}vs.hv curve[29]. The optical band gap of PANI/COF/BiOBr was reduced by about 0.37eV compared to BiOBr. The narrower band gap and higher photo-response were more favorable for photocatalytic degradation.

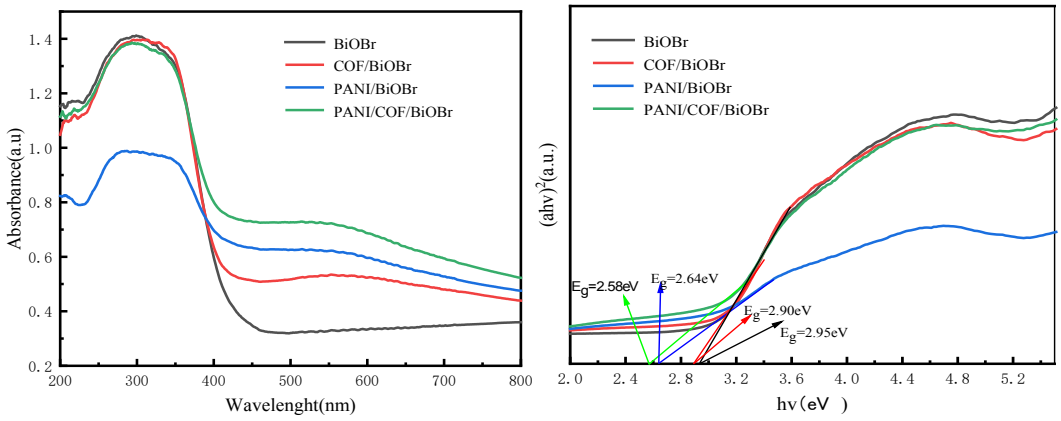

Fig. 5. (a) UV-Vis absorption spectra of BiOBr composites, and (b) (αhv) ^{2}vs.hv curves.

3.2. Photocatalytic properties of BiOBr composites

3.2.1. Degradation performance of Rhodamine B by BiOBr composites

The effect of degradation of Rhodamine B by BiOBr and its composites was shown in Fig. 6. It showed that the degradation rates of Rhodamine B by COF, PANI, BiOBr, COF/BiOBr, PANI/BiOBr, PANI/COF/BiOBr were 32.6%, 39.2%, 69%, 82.2%, 95.8% and 99.8%, respectively. It could be seen that the main BiOBr had a certain degradation effect, but the degradation effect of single COF or PANI was weak. After the addition of COF and PANI to the main BiOBr, the degradation effect of Rhodamine on the material was greatly improved, and the degradation rate of PANI/COF/BiOBr was significantly improved, which was 1.44 times that of the original BiOBr. The experimental results showed that PANI/COF/BiOBr showed a better effect on the degradation of Rhodamine B during the reaction time. It could conclude that the degradation effect of COF and PANI alone was not significant, so the following experiments discussed BiOBr, COF/BiOBr, PANI/BiOBr, PANI/COF/BiOBr materials. When the dye concentration was very low, the Langmuir-Hinshelwood linear fitting was performed, and the fitting formula was shown equation in (2) : where k was the first-order reaction rate constant. According to the slope of the fitted linear equation, the values k of COF, PANI, BiOBr, COF/BiOBr, PANI/BiOBr, PANI/COF/BiOBr were respectively: 0.00187 min^{-1}, 0.00244 min^{-1}, 0.00609 min^{-1}, 0.00925 min^{-1}, 0.01717 min^{-1}, 0.03503 min^{-1}. It also showed that PANI/COF/BiOBr composites had the best degradation rate to Rhodamine B

$$-In\frac{c_t}{c_0} = kt \tag{2}$$

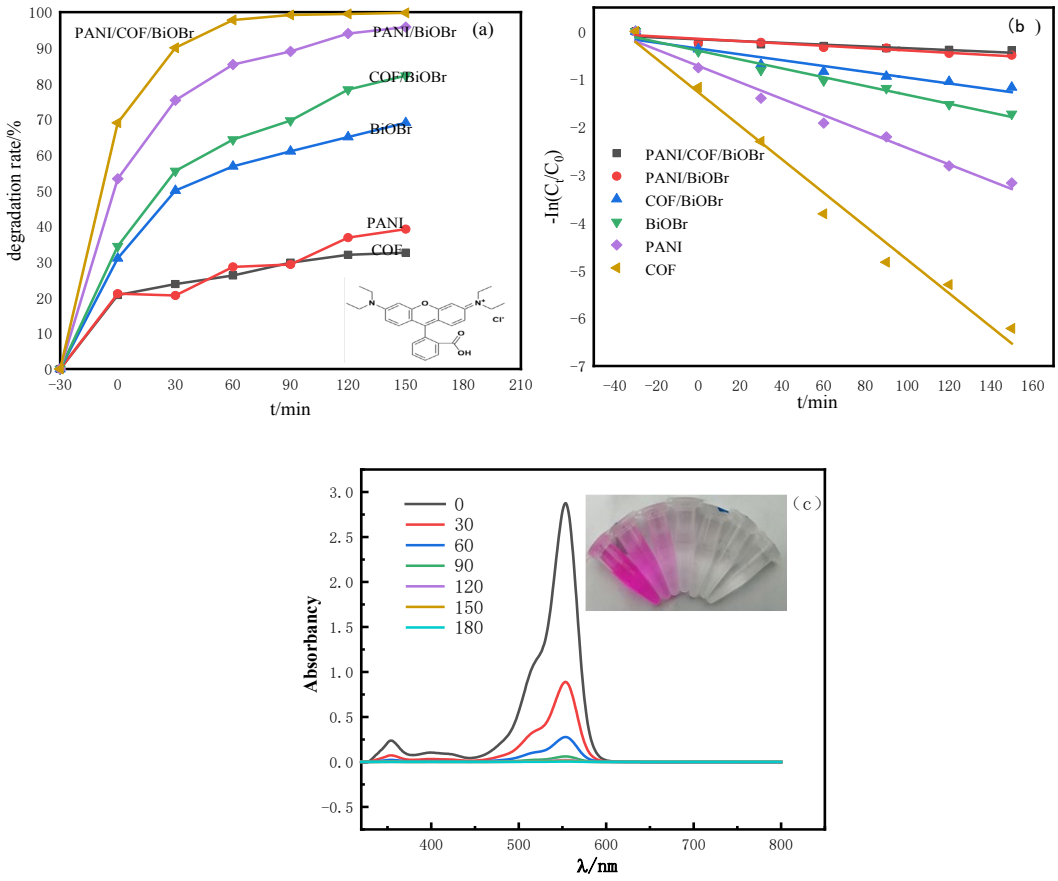

Fig. 6. Degradation diagram of Rhodamine B by BiOBr composites (a: degradation rate-time diagram; b: Langmuir-Hinshelwood linear fitting; c: Ultraviolet spectrum of Rhodamine B during degradation by PANI/COF/BiOBr).

3.2.2. The degradation performance of methylene blue and tetracycline by BiOBr composites

The degradation effect of BiOBr composites on methylene blue was showed in Fig. 7a. It showed that the degradation rate of methylene blue gradually increased with the increase of time. After 150 min of illumination, the degradation efficiency of methylene blue were 80.7%, 69%, 59.1% and 54.9%, corresponding to PANI/COF/BiOBr, PANI/BiOBr, COF/BiOBr and BiOBr, respectively. The degradation effect of PANI/COF/BiOBr on methylene blue was 1.47 times that of pure BiOBr.

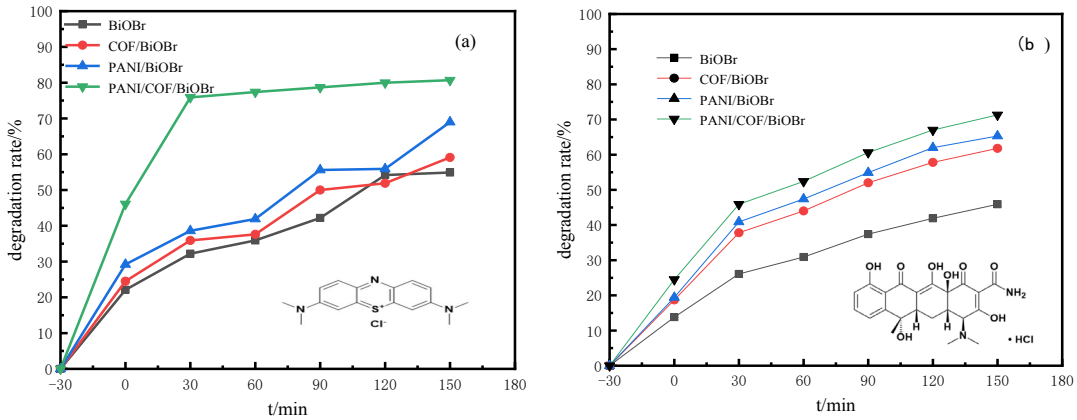

Fig. 7. Degradation effect of BiOBr composites on methylene blue (a) and tetracycline hydrochloride (b).

The degradation effect of BiOBr composites on tetracycline hydrochloride was shown in Fig.7b. It showed that the degradation rates of tetracycline hydrochloride were 45.9%, 61.8%, 65.3% and 71.3% after 150 minutes of illumination corresponding to BiOBr, COF/BiOBr, PANI/BiOBr,, PANI/COF/ BIOBr, respectively. The degradation effect of PANI/COF/BiOBr was best, which was 1.55 times that of pure BiOBr.

In the above experiments, it was found that Rhodamine B, methylene blue and tetracycline hydrochloride had different structures, but PANI/COF/BiOBr had better degradation effect on these organic compounds. It could be seen that PANI/COF/BiOBr had a certain universality to the degradation of organic matter. Combined with the solid UV diffuse reflection results of the material and the subsequent free radical quenching experiment, the reason may be that the addition of COF and PANI could increase the absorption of visible light, and separate the photogenerated electron-hole pairs effectively, reducing the recombination of electron-hole pairs and improving the photocatalytic activity.

3.3. Cycling performance of PANI/COF/BiOB

The cyclic degradation rate of Rhodamine B by PANI/COF/BiOBr was shown in Fig.8. As could be seen from the figure, the degradation rates of PANI/COF/BiOBr of three cycles were 98.6%, 92.6% and 68.4%, respectively. The degradation rate of the first and second cycles was more than 90%, but the degradation rate of the third cycle was reduced to 68.4%, meaning the degradation rate of PANI/COF/ BiOBr reduced by 30.63% after three cycles. XRD pattern of PANI/COF/BiOBr remain unchanged before and after cycling. The possible reason was that the composites degraded several times, the active site was covered by organic matter, and could not be eluted by simple acid-base treatment, so the cyclic performance was affected. However, in terms of the overall cycle efficiency, the cycle stability of PANI/COF/BiOBr was better.

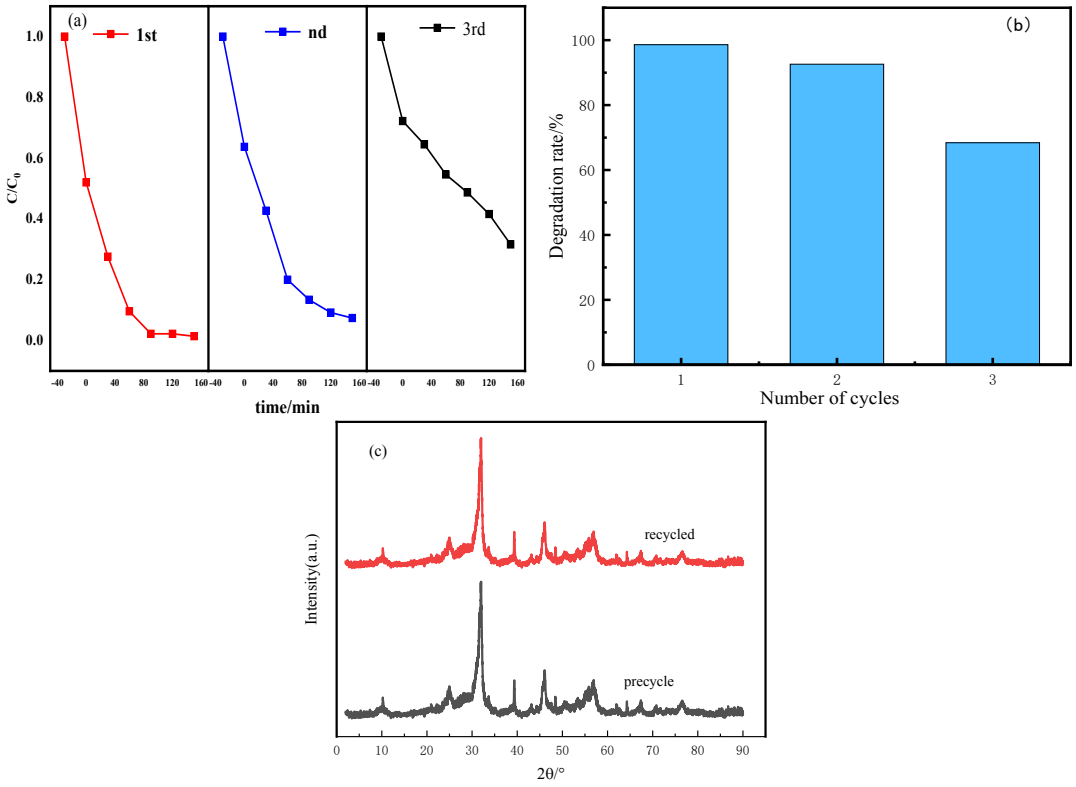

Fig. 8. Cyclic degradation of Rhodamine B by PANI/COF/BiOBr (a) column diagram of degradation rate (b) XRD pattern of PANI/COF/BiOBr before and after the cycles (c).

3.4. Photocatalytic mechanism of PANI/COF/BiOB

In order to further explore the effect of free radicals on Rhodamine B degradation and photocatalytic mechanism, the oxidation group capture experiment was carried out. As shown in Fig.9, when the concentration of quencher was 0.075 mol/L, the degradation rates of Rhodamine B solution by PANI/COF/BiOBr were 97.7%, 40.4%, 77.5%, 87.8% and 98.2%, respectively, corresponding to blank group solution, added sodium oxalate, silver nitrate, p-benzoquinone and isopropyl alcohol solution. It showed that the photocatalysis of free radicals in the photocatalysis process was as follows: $h^+ > e^- > \cdot O_2^- > \cdot OH$, indicating photogenerated holes (h^+) and photogenerated electrons (e^-) were the most active species in the photocatalytic process of Rhodamine B by PANI/COF/BiOBr. Combined with free radical capture experiments, the possible degradation mechanism of PANI/COF/BiOBr was proposed, as shown in Fig. 10. In the degradation process of PANI/COF/BiOBr materials, the main BiOBr mainly played the role of semiconductor, that was, h^+ and e- were generated in the process of illumination, and PANI and COF had a conductive synergistic effect, rapidly conducting and separating the generated h^+ and e^-, and most of the h^+ and e^- were directly involved in the degradation process of organic matter.

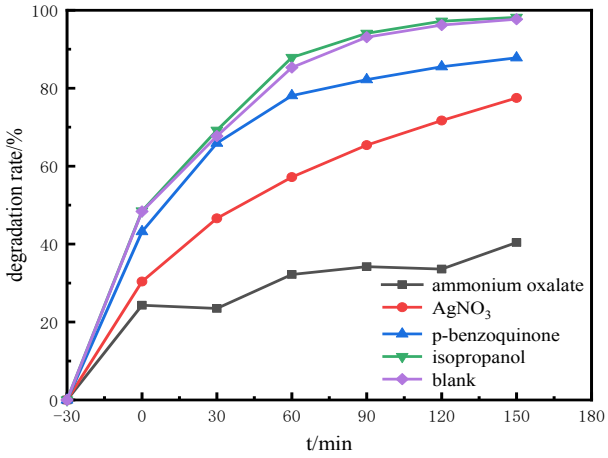

Fig. 9. Effect of quencher on degradation of Rhodamine B by PANI/COF/BiOBr.

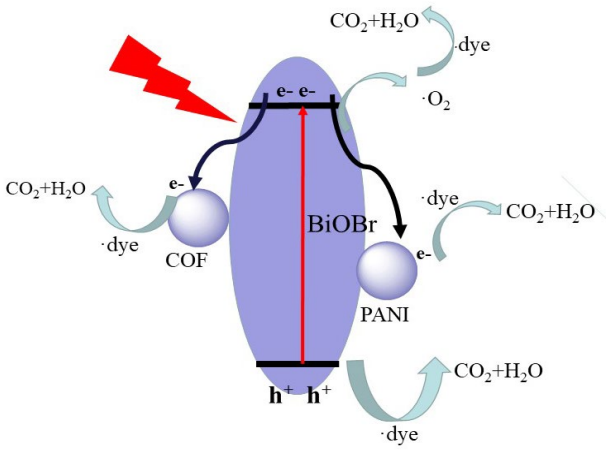

Fig. 10. Degradation mechanism diagram of PANI/COF/BiOBr.

4. Conclusion

BiOBr and its composites were synthesized by hydrothermal method using $Bi(NO_3)_3$ and CTAB as Bi and Br sources based on Schiff base reaction. The composites were characterized by XRD, SEM, FT-IR and DRS, and were used for photocatalytic experiments on Rhodamine B, methylene blue and tetracycline hydrochloride to study the degradation effect, catalyst stability and degradation mechanism. The experimental results showed that the main structure of PANI/COF/BiOBr composite was flower ball structure with tetragonal BiOBr crystal form, and the peak near at 520cm^{-1} was the infrared characteristic peak of BiOBr material, which corresponding to the Bi-O bond stretching vibration peak. The UV diffuse reflection results showed that the band gap energy of PANI/COF/ BiOBr decreased from 2.95eV to 2.58eV, and the absorption of visible light after 400nm was enhanced. The best catalysts for Rhodamine B, methylene blue and tetracycline hydrochloride degradation were PANI/COF/BiOBr materials, and the degradation rates were 1.44, 1.55 and 1.47 times of pure BiOBr, respectively.

The stability of PANI/COF/ BiOBr was good, and the degradation rate of PANI/COF/ BiOBr was reduced by 30.63% after three cycles. The free radical quenching experiment showed that photogenerated holes (h^+) and photogenerated electrons (e^-) were the most active species in the photocatalytic process.

Acknowledgements

The work was supported by Guangxi Provincial Natural Science Foundation of China (2020GXNSFBA297138); university-level scientific research project of Hechi University (2023XJZD004); Innovation and entrepreneurship training program for college students （S202210605029，S202310605003）

References

[1] F. R. Guo , J. C. Chen, J. Z. Zhao, Z. Chen , D. S. Xia , Z. L. Zha, Q. Wang, Chemical Engineering Journal 386,124014(2020); https://doi.org/10.1016/j.cej.2020.124014

[2] A. I. M. Asrai, M. H. Razali, K. A. M. Amin, U. M. Osman, Digest Journal of Nanomaterials and Biostructures 8(3), 1105, 1124(2023); https://doi.org/ 10.15251/DJNB.2023.183.1105

[3] Y. J. Peng, J. L. Lin, J. L Niu, X. L. Guo, Y. Z. Chen, T. K. Hu, J. H. Cheng, Y. Y. Hu, ACS Appl. Mater. Interfaces , 16(2), 2351−2364(2024); https://doi.org/10.1021/acsami.3c16037

[4] J. F. Zheng, X. Tang, C. Z. Fan, Y. C. Deng, X. M. Li, Q. Yang, D. B. Wang, A. B. Duan, J. Luo, Z. Chen, B. W. Zhang, Chem. Eng. J. 446(3), 136485(2022); https://doi.org/10.1016/j.cej.2022.136485

[5] Y. Guan, S. M. Wang, Q. D. Du, M. F. Wu, Z. Q. Zheng, Z.F. Li, S. C. Yan, J. Colloid Interface Sci., 624, 168-180(2022); https://doi.org/10.1016/j.jcis.2022.05.091

[6] Z. S. Li, G. H. Huang, K. Liu, X. K. Tang, Q. Peng, J. Huang, M. L. Ao, G.F, Zhang, J. Clean Prod., 272,122892(2020); https://doi.org/10.1016/j.jclepro.2020.122892

[7] M. M. Zhang, C. Lai, B. S. Li, D. L. Huang, G. M. Zeng, P. Xu, L. Qin, S. Y. Liu, X. G. Liu, H. Yi, M. F. Li, C. C. Chu, Z. Chen, J. Catal.,369 , 469-481 (2019); https://doi.org/10.1016/j.jcat.2018.11.029

[8] A. B. Geng, L. J. Xu, L . Gan , C. T. Mei, L. J. Wang, X.Y. Fang, M. R. Li, M. Z. Pan, S. G. Han, J.Q. Cui, Chemosphere, 250,126291(2020) ; https://doi.org/10.1016/j.chemosphere.2020.126291

[9] S. R. Zhu, Q. Qi , Y. Fang, W. N. Zhao, M. K.Wu, L. Han, Cryst. Growth Des. , 18 (2) : 883-891(2018); https://doi.org/10.1021/acs.cgd.7b01367

[10] R. Zhang, Q. Han, Y. Li, T. Q. Zhang, Y. Liu, K. L. Zeng, C. Zhao. Separation and Purification Technology, 234,116098(2020); https://doi.org/10.1016/j.seppur.2019.116098

[11] G. D. Fan, X. Li, X. L. Chen, Y. F. You, W. X. Dai, F. S. Qu, D. S. Tang, Z. S. Yan, Chem. Eng. J.,427, 132005(2020); https://doi.org/10.1016/j.cej.2021.132005

[12] A. P. Chowdhury, B. H. Shambharkar, Applied Organometallic Chemistry, 34(4) , 5436(2020); https://doi.org/10.1002/aoc.5436

[13] Y. L. Cai, Y. H. Xu, J. Z. Xiang, Z. Q. Zhang, Q. X. He, Y. F. Li, J. Lu. Journal of Environmental Sciences, 137, 321-332(2024); https://doi.org/10.1016/j.jes.2023.01.005

[14] Y. Liu, Z. F. Hu , J. C. Yu. Chemosphere, 278, 130376 (2021); https://doi.org/10.1016/j.chemosphere.2021.130376

[15] J. Y. Sun, S. D. Mo, Z. Zhang, J. H. Wen, D. G. Guo, Y. H .Li, L. Liu, Chem. Eng. J. 450,137980(2022); https://doi.org/10.1016/j.cej.2022.137980

[16] Z. S. Cai , J. B. Zhong, J. Z. Li, H. S. Jin, Inorganic Chemistry Communications, 126,108450(2021); https://doi.org/10.1016/j.inoche.2021.108450

[17] X. Q. Liu, L. Cai, Appl.Surf. Sci., 483, 875-887(2019); https://doi.org/10.1016/j.apsusc.2019.03.273

[18] Y. Zhang, L. Hu, H. H. Zhou, H. G. Wang, Y. C. Zhang, ACS Appl. Nano Mater. , 5(1). 391-400(2022); https://doi.org/10.1021/acsanm.1c03211

[19] X. M. Zhang, Q. Wang , Y. Liu, Chemical Engineering Journal, 475,14626(2023); https://doi.org/10.1016/j.cej.2023.146261

[20] H. Kaur, S. Kumar, S. Kaushal, R. Badru, P. P. Singh, A. Pugazhendhi, Environmental Research, 225, 114960(2023); https://doi.org/10.1016/j.envres.2022.114960

[21] V. A. Chhabra, R. Kaur, M. S . Walia, K. H. Kim, A. Deep, Environmental Research, 186, 109615(2020); https://doi.org/10.1016/j.envres.2020.109615

[22] Y. S. Qing, Y. X. Li , L. X. Cao, Y. J. Yang, L. Han, P. Dansawad, H. G. Gao, W. L. Li, Separation and Purification Technology, 314,123545(2023); https://doi.org/10.1016/j.seppur.2023.123545

[23] Y. G. Xu, Y. Ma, H.Y. Ji, S. Q. Huang, M. Xie, Y. Zhao, H. Xu, H. M. Li, Journal of Colloid and Interface Science, 537, 101-111(2019); https://doi.org/10.1016/j.jcis.2018.10.109

[24] H. Z. Zhang, J. J. Liu, Y. Zhang, B. Cheng, B. C. Zhu, L. X. Wang. Journal of Materials Science & Technology, 166, 241-249(2023);https://doi.org/10.1016/j.jmst.2023.05.030

[25] H. C. Xu, Y. Xu, Y. D. Wang, Q. M. Wang, Y. Y. Zhang, Q. B. Liao, K. Xi. ACS Appl. Nano Mater., 7, 3071−3081(2024); https://doi.org/10.1021/acsanm.3c05372

[26] Q. B. Liao, D. N. Wang, C. Ke, Y. Y. Zhang, Q.W. Han, Y. F. Zhang, K. Xi, Appl. Catal., B, 298,120548(2021); https://doi.org/10.1016/j.apcatb.2021.120548

[27] Q. J. Zhi, W. P. Liu, R. Jiang, X. N. Zhan, Y. C. Jin, X. Chen, X. Y. Yang, K. Wang, W. Cao, D. D. Qi, J. Z. Jiang, J. Am. Chem. Soc., 144, 21328-21336(2022); https://doi.org/10.1021/jacs.2c09482

[28] Y. Y. Zhao, H. X. Guo, J. Fan, J. Colloid Interface Sci. , 627, 180-193(2022); https://doi.org/10.1016/j.jcis.2022.07.046

[29] C. C. Wang, K. Rong , Y. P. Liu , F. Yang, S. L. Li . Science China materials, 67(2): 562-572(2024); https://doi.org/10.1007/s40843-023-2764-8